Supplemental Materials for

Anisotropy of Antiferromagnetic Domains in a Spin-orbit Mott Insulator

Longlong Wu[1*], Wei Wang[1], Tadesse A. Assefa[1,2], Ana F. Suzana[1], Jiecheng Diao[3], Hengdi Zhao[4], Gang Cao[4], Ross J. Harder[5], Wonsuk Cha[5], Kim Kisslinger[6], Mark P. M. Dean[1] and Ian K. Robinson[1,3†]

[1]*Condensed Matter Physics and Materials Science Department, Brookhaven National Laboratory, Upton, NY 11973, USA*

[2]*Stanford Institute for Materials and Energy Sciences, SLAC National Accelerator Laboratory, Menlo Park, California 94025, USA*

[3]*London Centre for Nanotechnology, University College London, London, WC1E 6BT, United Kingdom.*

[4]*Department of Physics, University of Colorado at Boulder, Boulder, Colorado 80309, USA*

[5]*Advanced Photon Source, Argonne, Illinois 60439, USA*

[6]*Center for Functional Nanomaterials, Brookhaven National Laboratory, Upton, New York 11793, USA*

[*]lwu@bnl.gov, [†]irobinson@bnl.gov

Supplemental Figures:

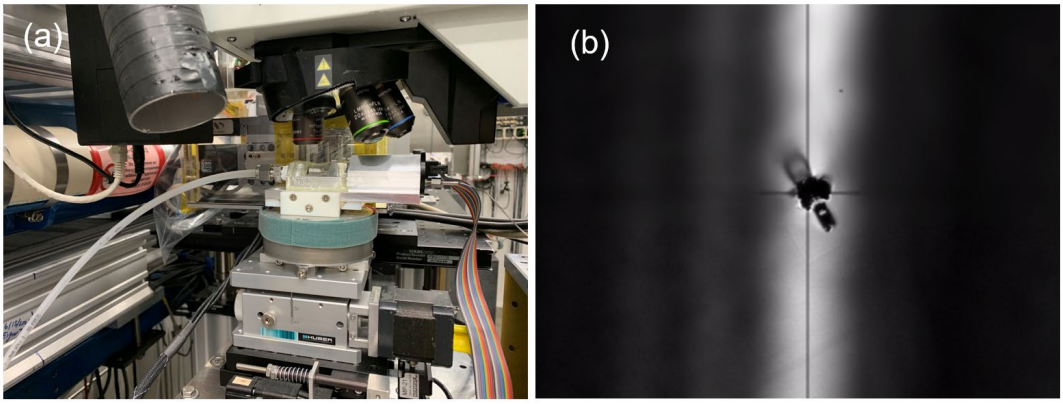

FIG. S1 Photographs of the experimental setup for the resonant Bragg coherent x-ray diffraction experiment. (a) Picture of the micro miniature refrigerator (MMR) stage during the BCDI experiment. (b) Sr_2IrO_4 sample under confocal microscopy at the 34-ID-C beamline.

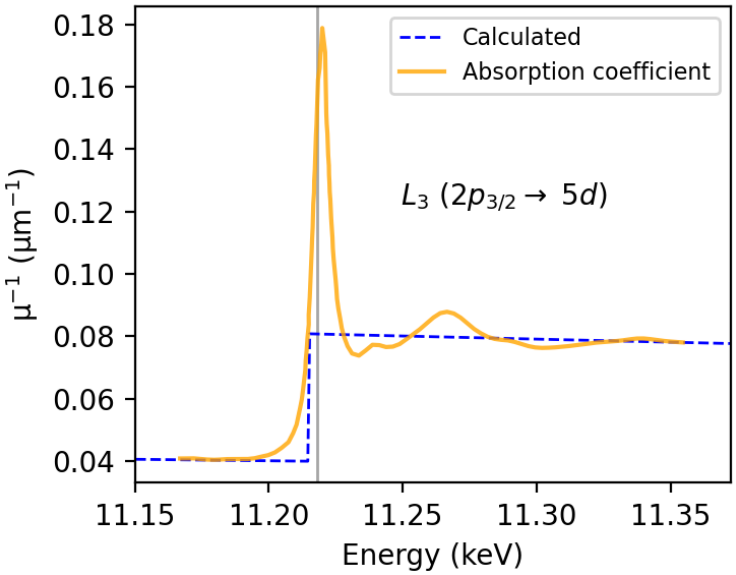

FIG. S2 Estimated x-ray penetration depth for the Sr_2IrO_4 sample. The estimation was completed by scaling the pre-edge and post-edge regions of the x-ray absorption coefficient with the calculated one as labeled by the blue dashed line [1,2]. The corresponding experimental x-ray absorption spectrum is obtained from Ref. [3]. Here, the grey line shows the position of the resonance (11.218 keV), which is found to maximize the intensity of the resonant x-ray magnetic scattering from the sample.

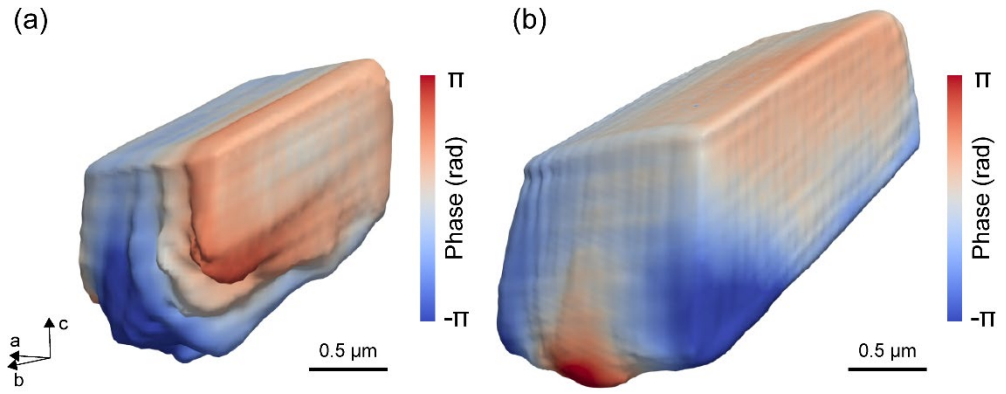

FIG. S3 Comparison of reconstructed Sr_2IrO_4 structure from two different samples prepared by Focused Ion Beam (FIB) milling method, separately. (a) Isosurface of the Sr_2IrO_4 sample reconstructed from the (116) peak of the crystal, as the corresponding SEM image shown in Fig 1. (b) Isosurface of another Sr_2IrO_4 sample from the (116) peak. Here the two samples were prepared with the same method but with slightly different sizes. For both crystals, near the bottom, a larger strain is shown, which is probably induced by a larger beam current (i.e., ~2.4 nA) for the bulk milling of the Sr_2IrO_4 sample (see FIB Sample Preparation section for details). After bulk milling, the bottom region is welded directly to the Pt and its larger strain is retained, while the top and sides were polished with low beam current.

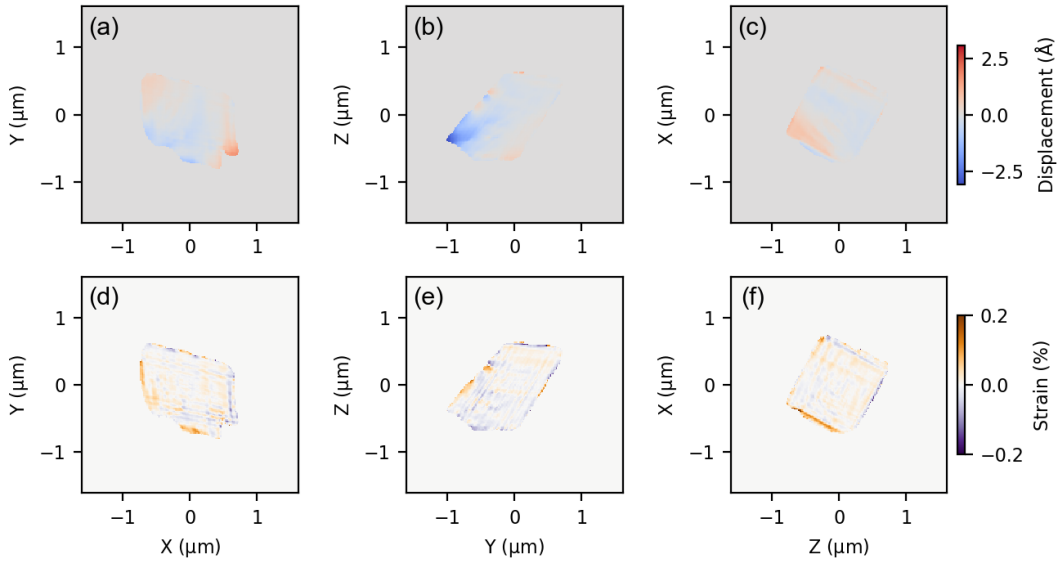

FIG. S4 Calculated strain inside the Sr_2IrO_4 crystal by using the (116) peak. Central slice of the displacement distribution (a) perpendicular to the **Q** vector [i.e., (116) peak]. (b)-(c) along the **Q** vector. (e-f) Corresponding strain distribution.

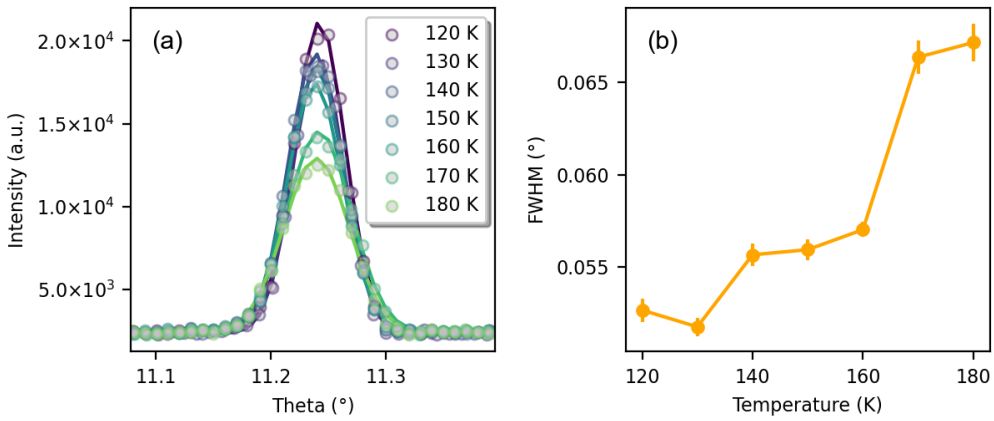

FIG. S5 (a) Representative rocking curves of antiferromagnetic (106) Bragg reflection measured from an ~8 μm Sr_2IrO_4 crystal as a function of the crystal temperature. Here, the dots represent the experimental data, and the lines represent the corresponding fitted results with Pseudo-Voigt function. (b) Extracted full width at half maximum (FWHM) of the antiferromagnetic (106) peak from (a).

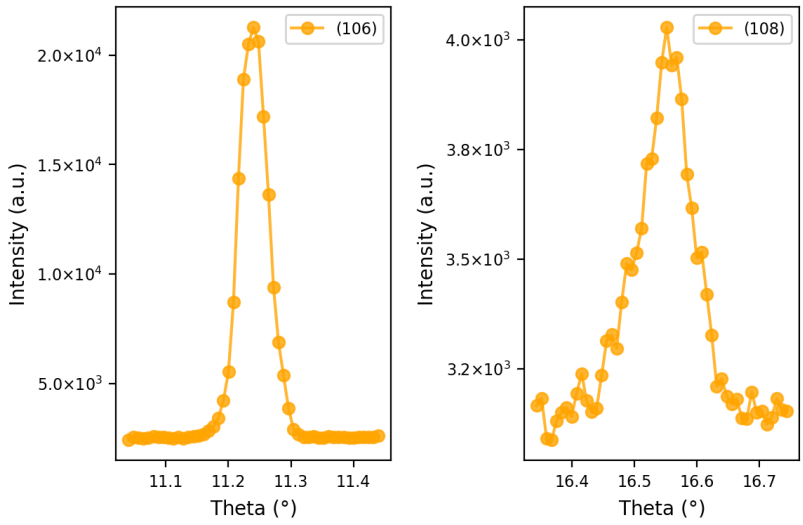

FIG. S6 Representative rocking curves of antiferromagnetic Bragg reflections at (106) and (108) from an ~8 μm Sr_2IrO_4 single crystal prepared by the FIB lift-out method. Both measurements are obtained at 120 K.

Supplemental Methods:

Sr_2IrO_4 Crystal Growth:

The high-quality Sr_2IrO_4 single crystal was grown from off-stoichiometric quantities of $SrCl_2$, $SrCO_3$, and IrO_2 using self-flux techniques [4]. The corresponding molar ratio for the materials is 1.8:1.0:15. The mixture was melted at 1300 ℃ and subsequently cooled down to 900 ℃ at a rate of 8 ℃ per hour before being furnace-cooled to room temperature.

FIB Sample Preparation:

After the crystal was grown, to prepare a micro-size Sr_2IrO_4 crystal with a well-defined shape for Bragg coherent x-ray diffraction experiments, the large Sr_2IrO_4 crystal was pre-oriented crystallographically using a Laue diffractometer. After alignment, its [001] crystal direction was along the vertical direction and the [110] crystal direction was along the horizontal direction. The tetragonal unit cell with a = b = 5.49 Å and c = 25.8 Å at room temperature was used to index the reciprocal space.

During the sample preparation using Focused Ion Beam (FIB) method, the FIB lift-out protocol was then used to cut a micro-size Sr_2IrO_4 sample from the corresponding large crystal [5]. First, a 1 μm thick sacrificial platinum cap was deposited over the implanted surface of the Sr_2IrO_4 by electron beam assisted deposition. After the platinum deposition, a lift-out sample, similar to that used for TEM or atom probe tomography, was prepared using a Helios G5 Dual Beam SEM/FIB Microscope. A 30 keV Ga ion beam with 2.4 nA and 9.1 nA beam current was applied for the bulk milling of the Sr_2IrO_4 sample. After this, a ~5×5×5 μm^3 sized sample was extracted/lifted from the bulk using Omniprobe needle, and the cube sample was attached to a 1×1 cm^2 silicon wafer using a platinum weld. Then, the lifted Sr_2IrO_4 sample was trimmed down to a size of approximately 1.2

μm in each direction using lower beam voltages (30 keV, 16 keV, 8 keV, and 5 keV) and smaller beam currents (0.26 nA, 0.12 nA, 63 pA, and 61 pA). Finally, one keV low-energy final cleaning was used to clean off the surface damage from the previous FIB milling step. Such preparation eliminates most of the damage from previous FIB milling steps.

BCDI Experiments:

The Bragg coherent x-ray diffraction experiments were carried out at the 34-ID-C beamline of the Advanced Photon Source. A double crystal monochromator was used to select the energy of 9.0 keV and Kirkpatrick–Baez mirrors were used to focus the beam to 600 × 600 nm^2. To fully illuminate the crystal for valid Bragg coherent x-ray imaging, the beam size was adjusted to $2.2 \times 1.4\ \mu m^2$ (H×V) by changing the coherence-defining entrance x-ray slit to $10 \times 20\ \mu m^2$ (H×V). The sample was mounted on a micro miniature refrigerator (MMR) stage for BCDI measurements, where the temperature of the sample was controlled precisely by an MMR K-20 controller under a fixed flow of nitrogen gas. Since the Sr_2IrO_4 sample was pre-aligned before FIB preparation, the precise crystal alignment was quickly determined by using the (204) and (116) peaks of the sample, with a six-axis diffractometer to maneuver the sample orientation. During alignment, the energy of the incident x-ray was 9 keV. After the Sr_2IrO_4 crystal was well aligned, the energy of the incident x-ray beam was tuned to 11.218 keV, which was found to maximize the intensity of the resonant x-ray magnetic scattering. During the measurements, the resonant x-ray magnetic BCDI data were collected by rocking the sample around the (116) and (106) peaks, separately. The corresponding diffraction signal was collected by a Timepix photon-counting detector mounted 2.5 m away from the Sr_2IrO_4 sample, and a vacuum flight tube was used to avoid air scattering contribution in the diffraction signal.

BCDI Data Reconstruction:

Before feeding the Bragg coherent x-ray diffraction data into a phase retrieval algorithm [6-8] developed in Python, the white-field correction, dark background removal, and hot pixel removal were applied. When applying the phase retrieval algorithm, the measured Bragg 3D diffraction patterns (in detector coordinates) were used as input to the iterative phase-retrieval scheme to reconstruct their corresponding real-space structure information. During the reconstruction, the initial support size of the particle in real space was half the size of the input diffraction pattern array in each dimension. The algorithm was started with 200 steps of relaxed averaged alternating reflection (RAAR). Then, it was switched between hybrid input-output (HIO) with β=0.9 and error reduction (ER) after every 50 iterations. After the first 100 iterations, the shrink-wrap method was applied in real space to dynamically update the support every ten iterations [9]. At the end of the reconstruction, 200 steps of error reduction were used. The total number of iterations was 1800. After the reconstruction, all the reconstructed results were converted from the detector to sample coordinates. The computation was performed on a computer with 196 GB of RAM and two NVIDIA RTX A5000 GPUs.

Lattice Strain Calculation:

For a single Bragg peak, there is a simple linear relationship between the observed image $\phi(\mathbf{r})$ phase and the crystal displacement field $\mathbf{u}(\mathbf{r})$: $\phi(\mathbf{r}) = \mathbf{Q} \cdot \mathbf{u}(\mathbf{r})$ [10]. The strain is related to the variation of the *d*-spacing of the Sr_2IrO_4 crystal based on the measured Bragg peak. For the Sr_2IrO_4 crystal (116) peaks, the strain can be calculated as: $\epsilon_{106} = \frac{\partial u_{106}}{\partial x_{106}}$, where u_{106} is the corresponding displacement field.

References:

[1] M. P. Dean, G. Dellea, R. S. Springell, F. Yakhou-Harris, K. Kummer, N. B. Brookes, X. Liu, Y. J. Sun, J. Strle, T. Schmitt, L. Braicovich, G. Ghiringhelli, I. Bozovic, and J. P. Hill, Persistence of magnetic excitations in $La_{2-x}Sr_xCuO_4$ from the undoped insulator to the heavily overdoped non-superconducting metal, Nat. Mater. **12**, 1019 (2013).

[2] D. Paganin, *Coherent X-ray optics* (Oxford University Press, 2006).

[3] D. Haskel, G. Fabbris, M. Zhernenkov, P. P. Kong, C. Q. Jin, G. Cao, and M. van Veenendaal, Pressure tuning of the spin-orbit coupled ground state in Sr_2IrO_4, Phys. Rev. Lett. **109**, 027204 (2012).

[4] G. Cao, J. Bolivar, S. McCall, J. E. Crow, and R. P. Guertin, Weak ferromagnetism, metal-to-nonmetal transition, and negative differential resistivity in single-crystal Sr_2IrO_4, Phys. Rev. B **57**, R11039 (1998).

[5] T. A. Assefa, Y. Cao, J. Diao, R. J. Harder, W. Cha, K. Kisslinger, G. D. Gu, J. M. Tranquada, M. P. M. Dean, and I. K. Robinson, Scaling behavior of low-temperature orthorhombic domains in the prototypical high-temperature superconductor $La_{1.875}Ba_{0.125}CuO_4$, Phys. Rev. B **101** (2020).

[6] L. Wu, S. Yoo, A. F. Suzana, T. A. Assefa, J. Diao, R. J. Harder, W. Cha, and I. K. Robinson, Three-dimensional coherent X-ray diffraction imaging via deep convolutional neural networks, npj Computational Materials **7** (2021).

[7] L. Wu, Y. Shen, A. M. Barbour, W. Wang, D. Prabhakaran, A. T. Boothroyd, C. Mazzoli, J. M. Tranquada, M. P. M. Dean, and I. K. Robinson, Real Space Imaging of Spin Stripe Domain Fluctuations in a Complex Oxide, Phys. Rev. Lett. **127**, 275301 (2021).

[8] L. Wu, P. Juhas, S. Yoo, and I. Robinson, Complex imaging of phase domains by deep neural networks, IUCrJ **8**, 12 (2021).

[9] S. Marchesini, H. He, H. N. Chapman, S. P. Hau-Riege, A. Noy, M. R. Howells, U. Weierstall, and J. C. H. Spence, X-ray image reconstruction from a diffraction pattern alone, Phys. Rev. B **68** (2003).

[10] I. Robinson and R. Harder, Coherent X-ray diffraction imaging of strain at the nanoscale, Nat. Mater. **8**, 291 (2009).